TURBULENT ENTRAINMENT FROM A TURBULENT BACKGROUND

K.S. Kankanwadi
Department of Aeronautics
Imperial College London
South Kensington Campus, London, UK
krishna.kankanwadi12@imperial.ac.uk

O.R.H. Buxton
Department of Aeronautics
Imperial College London
South Kensington Campus, London, UK
o.buxton@imperial.ac.uk

ABSTRACT

Simultaneous particle image velocimetry (PIV) and planar laser induced fluorescence (PLIF) measurements were conducted in order to investigate the effects of background turbulence on the entrainment process as well as on the behaviour of the wake interface. Previous studies have highlighted the importance of length scale as well as turbulence intensity in the background flow. This paper reports on a parametric study examining entrainment into the wake of a circular cylinder by independently varying background turbulence parameters through the use of turbulence generating grids. Despite the availability of turbulent rotational fluid on both sides of the interface, the classical turbulent/non-turbulent interface result of an enstrophy jump is reproduced, even in the harshest incoming free-stream turbulence conditions. Examining the tortuosity, reveals that both length scale and turbulence intensity in the background turbulence act to increase the interface surface area. Furthermore, the entrainment process is found to be greatly sensitive to the turbulence intensity of the subjected free-stream turbulence. However, despite an increase in surface area, a net reduction in mean entrainment mass flux is observed with increased intensity in the background turbulence. Examining the mass flux PDFs, reveals that this behaviour is a result of substantial, yet infrequent detrainment events.

INTRODUCTION

Turbulent entrainment is the process by which mass is transferred into a body of turbulent fluid from the background. This process is of great significance as it defines the growth rate of regions encompassing turbulent fluid. Applications of this process are widespread and range from the growth of a volcanic plume to the spread of an oil spill in an ocean. The rate of entrainment is effectively set by the flow dynamics near the outer boundary of these regions. The outer boundary is characterised by a sharp contorted interface of finite thickness. When surrounded by irrotational flow, this boundary is referred to as the turbulent/non-turbulent interface (TNTI), and has been studied to a great extent at the edges of wakes, jets, mixing layers and boundary layers. The pioneering work of Corrsin & Kistler (1955), made great strides into understanding the nature of the TNTI. They postulated the existence of a viscous 'superlayer' (VSL), a zone where viscosity plays a central role in acting to transmit vorticity that is always present within the turbulent portion of the flow, to the irrotational part of the flow. They further proposed that the propagation velocity of this layer is defined by the molecular viscosity, ν, and the rate of straining of the flow ($\sim \varepsilon/\nu$). Where ε is the dissipation rate of turbulent kinetic energy. Hence, suggesting the local entrainment rate here is governed by the Kolmogorov velocity, u_η (note, $u_\eta = (\varepsilon\nu)^{1/4}$). These scalings have since been experimentally confirmed by Holzner & Lüthi (2011), who analysed a turbulent front generated by an oscillating grid.

A significant amount of work has gone into understanding the TNTI as well as entrainment from a non-turbulent environment. However, the process of entrainment when the background itself is turbulent is largely unexplored and poorly understood. A clear understanding is necessary as a majority of industrial and environmental flows exist in a turbulent background. Literature on turbulent-turbulent entrainment (TTE) is very scarce and only a few studies have examined it. Previous studies have highlighted the importance of two parameters of the free-stream turbulence to TTE, $\{L,\ u'\}$, respectively, the length scale and turbulence intensity.

Gaskin *et al.* (2004) investigated the near field of plane jets in a turbulent environment. They observed that once the turbulence intensity in the background was strong enough to disrupt the energy-containing eddies of the jet, the entrainment mechanism switched from large-scale engulfment to the small-scale process of turbulent diffusion. In this case the result was a suppressed rate of entrainment as a result of the background turbulence. Ching *et al.* (1995) also associated the dominant parameter to be u' in the free-stream turbulence (FST). In a study that observed turbulent line plumes subjected to FST, they were able to show a marked change in spreading of the plume when the plume convective velocity, w_* was comparable to the background turbulence intensity. They were also able to show that the plume was destroyed from the onset when $u' > w_*$.

Eames *et al.* (2011), on the other hand, demonstrated the influence of L, on the spreading rate of a cylinder wake. They concluded that in the absence of FST, the wake grew diffusively with respect to $x^{1/2}$, where x is the streamwise distance downstream of the cylinder. However, when FST was introduced and the velocity deficit had sufficiently decayed that it was comparable to u' of the ambient turbulence, Eames *et al.* explained that the wake grew linearly when L was larger than the wake width. If this condition was not met, the wake continued to grow diffusively.

It is clear to see from current literature that L and u' both have a part to play in the physics behind TTE. Although there is no consensus on the influence of each parameter and their respective sensitivities. A systematic investigation exploring the effects of these parameters is being conducted in this study through the investigation of a wake behind a cylinder under the influence of free-stream turbulence, in which these properties may be varied independently of each other.

METHODOLOGY

To this end simultaneous PIV and PLIF experiments have been conducted in a water flume located at Imperial College London. Reynolds numbers based on the diameter (d) of the circular cylinder, Re_d, of approximately 12000 & 4000 were achieved, hence, placing the flow around the cylinder in the sub-critical regime. Due to the fact that rotational flow is present on both sides of the interface a high Schmidt number scalar is injected into the wake from the rear face of the cylinder in-order to demarcate the wake from the free-stream. Tests conducted in a non-turbulent background comparing the extent of the scalar to the enstrophy distribution, confirm that the released scalar does indeed mark the wake fluid. This paper examines the entrainment process and the turbulent interface through a high resolution simultaneous planar-PIV and PLIF experiment approximately 40 diameters downstream of a circular cylinder. The scalar boundary is used to identify the location of the interface, from which conditonal statistics are calculated. The process of interface identification and the processing steps to evaluate the entrainment mass flux are described in the sections below.

Interface identification and treatment

The metric used for interface identification in this paper relies on the gradient of the light intensity present in the PLIF image. A simple light intensity threshold is not sufficient, since doing so assumes a consistent ejection of the dye at the nominal concentration along with a consistent power output from the laser source. These conditions are not usually met and result in a few eddies being illuminated with a greater brightness than others in the same field of view (FOV). Furthermore, a 'halo' effect caused by secondary fluorescence of the dye results in illumination of regions around bright parts of the dye. This problem is highlighted and algorithmically resolved by Baj *et al.* (2016). However, due to the nature of this phenomenon the 'halo' regions present a gradual increase in light intensity around bright parts of the dye. Hence, to avoid false detections, an identification metric that utilises the light intensity gradient as its input, was deemed to be appropriate. This is mathematically defined as, $|\nabla\phi|$, where, ϕ is the light intensity of the PLIF image. Figure 1 depicts a typical image and the identified interface. The `contour` function in Matlab is used to identify the longest continuous contour that satisfies the chosen threshold on the gradient metric. Similar to the interface treatment methodology of Mistry *et al.* (2016), pockets of the wake that are present in the free-stream (as seen in the top right corner of figure 1) are not considered in any further calculations. The ensemble of points that are used for conditional analysis arrive from regions along an interface contour that satisfy a condition, which prevents it from doubling back on itself. For each x-position, the contour is only allowed to exist in a single y location. In the case when multiple y-positions exist for a single x-position, only the data-point that is furthest away from the turbulent core is used. This creates an 'envelope' of the interface and defines the ensemble of points used for further analysis.

As with any study that utilises a threshold based method for interface identification, it is necessary to conduct a sensitivity study in order to appropriately select the threshold that faithfully identifies the interface. Figure 2 plots the mean value of enstrophy available in the regions not considered to be part of the wake for respective threshold values. Note that this result is for the test case of no grid, that is a TNTI, where we would expect to find minimal out of wake enstrophy. A distinct jump is clear to see and the solid red line represents the chosen threshold value.

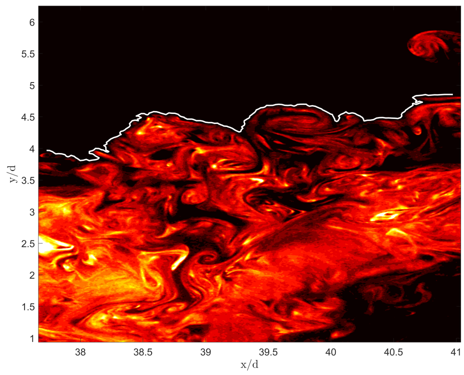

Figure 1: A typical PLIF image. The solid white line represents the interface as identified by the gradient metric.

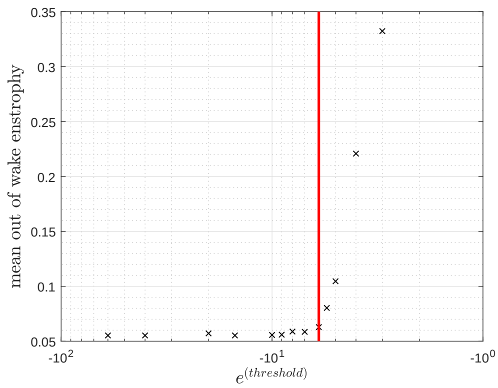

Figure 2: Threshold sensitivity study showing the mean normalised enstrophy considered to be outside of the wake for varying gradient threshold values.

Entrainment flux calculation

The motion of the interface is governed by two distinct phenomena. On the one hand, local fluid is advecting turbulence in space, whereas fluid from the background is also being entrained into the wake and causing it to grow in size. The latter is controlled by the local entrainment velocity, $\mathbf{V}_\gamma$, the calculation of which, requires the knowledge of both the time-resolved instantaneous location of the interface as well as the background fluid velocity. The process to evaluate the entrainment velocity is similar to the one used by Mistry *et al.* (2016) and the steps are listed below. Figure 3 graphically depicts the process.

1. Local fluid velocity u_0: The local fluid velocity is interpolated from the nearest grid point for each point along the contour at time t_0 (see figure 3a).
2. Advection subtraction: Contour at time, t_1, ($\mathbf{C}_1$), is identified and subtracted for local advection. Each point in $\mathbf{C}_1$ is subtracted by the vector $\Delta t\mathbf{u}_0$, where Δt is the time interval between two snapshots (see figure 3b).
3. Entrainment velocity: The difference between the original contour, $\mathbf{C}_0$, and the advected contour, $\mathbf{C}_1 - \Delta t\mathbf{u}_0$, is used to calculate an interface difference velocity vector. The normal component of this vector with respect to $\mathbf{C}_0$, is the entrainment velocity, $\mathbf{V}_\gamma$.

Integrating the entrainment velocity along the interface produces a value for the mass flux entrained into the wake (see eqn. (1)). Note that this value is normalised by the cylinder diameter, d, and the incoming free-stream velocity, U_∞. Since, the fluid in the flume is incompressible, the density term has been neglected from the equation below.

$$Normalised\ Mass\ Flux = \frac{1}{d \times U_\infty} \int_0^s V_\gamma . d\xi \qquad (1)$$

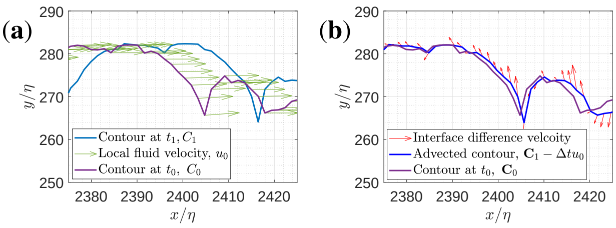

Figure 3: Plots depict the entrainment velocity calculation process. Note that η represents the Kolmogorov length scale.

RESULTS AND DISCUSSIONS

The effects of FST are two-fold. On the one hand, the near field is affected as the shedding mechanism of the cylinder is disrupted by the incoming turbulence. Additionally, L and u' in the free-stream, also have a direct affect on entrainment into the wake, downstream of the near wake region. This paper will focus on the latter, although our wider work also considers the former.

Experiments were conducted in the far wake ($37 \leq x/d \leq 41$) in order to quantify the effects of free-stream turbulence on the entrainment process. A circular cylinder of diameter, $d = 10$ mm, was used for this purpose, at a Reynolds number of, $Re_d \approx 4000$. Figure 4 illustrates the free-stream turbulence parameter envelope of this study. Note that background free-stream turbulence intensity of the facility is equal to 1.4%, and is representative of the amount of residual turbulence intensity in our control case ('no grid' Run 17). Figure 5 presents the transverse correlation function for the stream-wise fluctuating velocity, R'_{12}, in the bulk flow. Calculating the integral length scale for 'no grid' is not straightforward due to the presence of velocity correlation over a large distance. However an estimate for the integral length scale can be calculated by fitting an exponential to the short range correlation peak, producing a length scale estimate, L_{12}, of 3.4 mm. The 8 remaining runs span a turbulence intensity, TI, space from 2% to 14%, with length scales varying up to 2.6 cylinder diameters. Both TI and L_{12} are defined in the equations 2 and 3 respectively. Note that the the correlation function is integrated from zero to $\hat{r}$, where $\hat{r}$ is the location of the first zero crossing of the correlation function.

$$TI = \frac{(u'^2 + v'^2)^{1/2}}{U_\infty} \qquad (2) \qquad\qquad L_{12} = \int_0^{\hat{r}} R'_{12} dr \qquad (3)$$

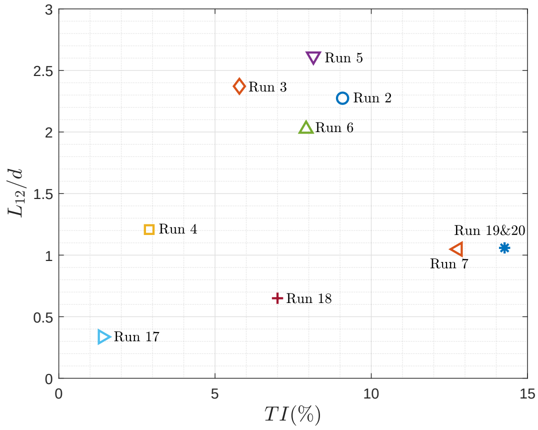

Figure 4: Free-stream turbulence parameter envelope

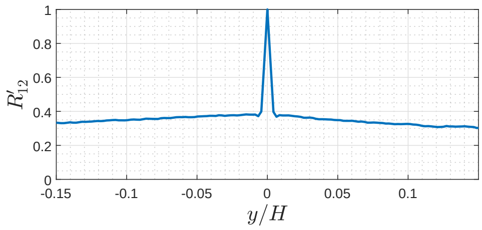

Figure 5: Transverse correlation function for stream-wise fluctuating velocity. Note, H represents the width of the flume's working section.

Interface conditioned statistics

Figures 6 and 7, depict normalised enstrophy and streamwise velocity as a function of distance normal to the wake boundary (γ). (Note that the wake boundary is analogous to the turbulence/irrotational boundary in the case of a TNTI and is defined as the edge of the scalar extent. It corresponds to $\gamma = 0$.) The no-grid control case reproduces expected behaviour for both interface conditioned enstrophy as well as the streamwise velocity jump (da Silva *et al.*, 2014). The base level of enstrophy rests at a non-zero value in the free-stream. This is as a result of the residual free-stream turbulence present in the facility. With the introduction of background turbulence, we find that the classical TNTI result of an enstrophy jump at the interface is still present when turbulence is available on both sides of the interface. Hence, analogous to the TNTI, there exists a turbulent/turbulent interface where enstrophy adjusts between the two fluid regions. As expected, the base level of enstrophy, as seen on the free-stream side of the interface, increases with added background turbulence intensity. For a majority of the grid turbulence cases, an extension to the enstrophy delta across the interface is seen. When the background turbulence becomes extreme, as is the case for runs 7, 19 and 20, an enstrophy jump is still present, although the enstrophy delta across the interface reduces in size as a severe increase is observed in the enstrophy available in the free-stream side of the interface.

Figure 7 depicts the stream-wise velocity jump across the interface. As long as the turbulence isn't too overpowering, an increase in the shear rate by 86% relative to the no-grid case is observed at the turbulent-turbulent interface. This value represents the mean increase in linear gradients that are evaluated by fitting to data-points that reside inside the wake ($\gamma/d < 0$). When rotational fluid is available on both sides of the interface, we expect the only consistent 'marker' of the wake to be time-averaged low momentum fluid. However in runs 7, 19 and 20 this property is no longer seen due to strong wakes also being present in the background. Despite the clear loss of a mean-momentum jump across the interface in these cases, it is interesting to observe that an enstrophy jump is still present even though the turbulence intensity in the free-stream is higher than in the wake. The geometry of these cases will be explained further in the following sections.

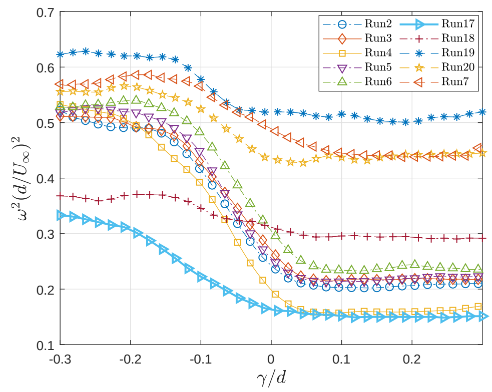

Figure 6: Normalised enstrophy as a function of normal distance away from the wake boundary.

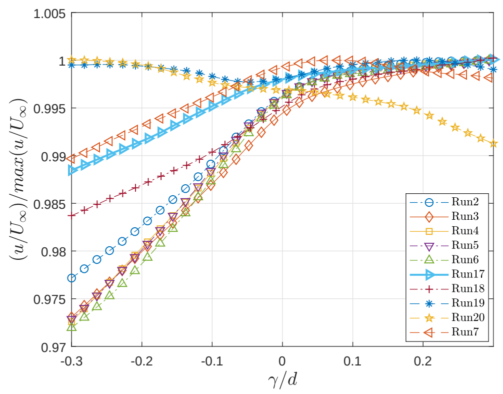

Figure 7: Normalised mean velocity as a function of normal distance away from the wake boundary.

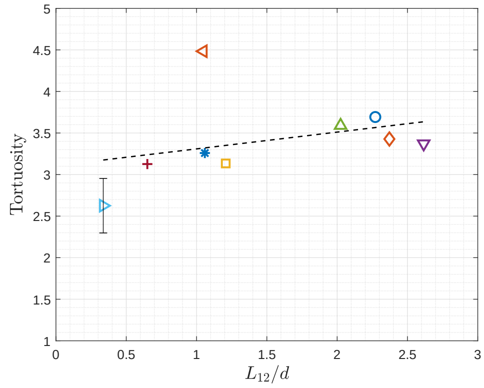

Figure 8: Plot depicts the variation of interface tortuosity as a function of subjected turbulence's integral length scale. The dashed line indicates a linear regression fit. The single error bar represents 10 times the 95% confidence interval. Other error bars have been omitted as all confidence intervals are very narrow.

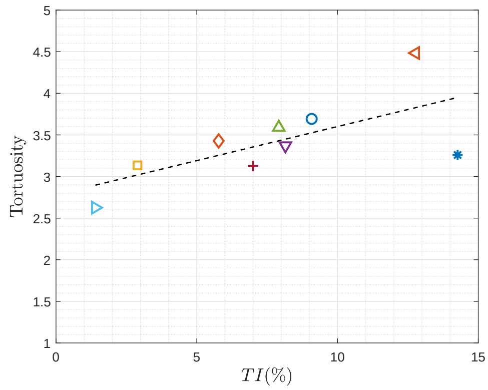

Figure 9: Plot depicts the variation of interface tortuosity as a function of subjected turbulence intensity. The dashed line indicates a linear regression fit.

Tortuosity

Tortuosity defines the level of contortion of the interface. Mathematically, this is the ratio of the length of the wake boundary to the distance between its two ends. A sensitivity study to the input parameters reveals the dependence on both parameters for the tortuosity value. An increase in either parameter, the background turbulence intensity or the length scale, both result in a more tortuous interface. Figures 8 and 9, display the near linear correlation with respect to subjected integral length scale and turbulence intensity. Reviewing the PDFs (figure 10) shows wider peaks that are shifted to the right, in the presence of any incoming grid turbulence, highlighting the prevalence of intermittent high magnitude events along with a modal shift towards a higher tortuosity value. Hence, this result goes on to suggest an increased interface surface area with added background turbulence.

Entrainment mass flux

Entrainment flux is calculated as a mean over the entire ensemble for each turbulence case and the behaviour is examined against the input turbulence parameters. Figure 11,

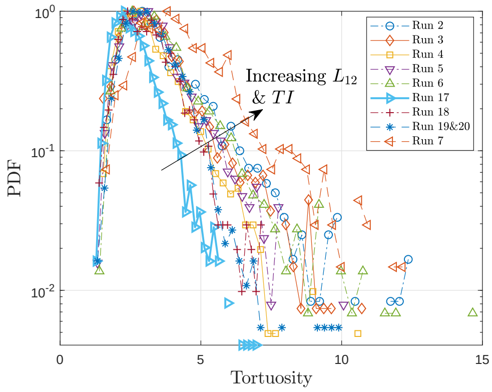

Figure 10: Probability density function for interface tortuosity for all subjected turbulence cases.

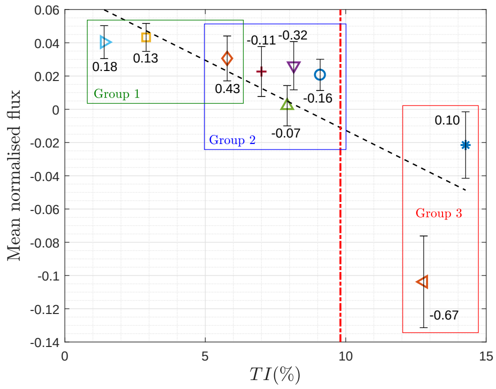

Figure 11: Entrainment mass flux as a function of subjected free-stream turbulence intensity (positive value indicates entrainment into the wake from the background). The dashed line indicates a linear regression fit with a coefficient of determination of 0.58. Text next to each datapoint indicates the skewness of the respective dataset.The error bars represent a 95% confidence interval. The red dot-dashed line indicates the turbulence intensity near the centerline of the wake.

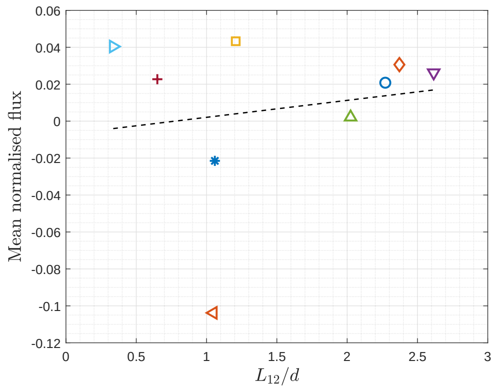

Figure 12: Entrainment mass flux as a function of subjected free-stream integral length scale (positive value indicates entrainment into the wake from the background). The dashed line indicates a linear regression fit with a coefficient of determination of 0.03.

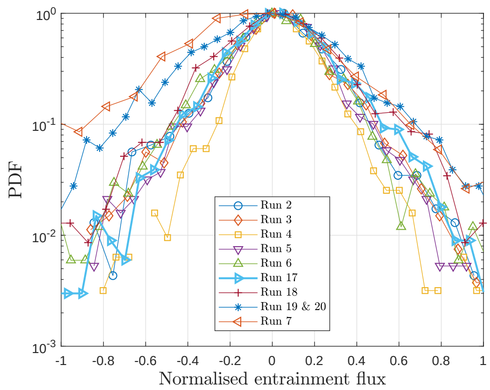

Figure 13: Probability density function for entrainment flux for all subjected turbulence cases.

depicts the variation of the mean flux with input turbulence intensity. A negative correlation can be observed, leading to an assertion that an increase in background turbulence intensity acts to reduce the rate at which background fluid is entrained into the wake in a mean sense. This seems to be an unintuitive progression, following on from the tortuosity result. We observe a reduction in entrainment flux depsite the increased interface surface area (due to increased tortuosity) when the cyldner is subjected to incoming grid turbulence. However, an explanation can be attained by examining the probability density function of the normalised flux (see figure 13). The collection of subjected turbulence cases can be split into three groups. Group 3 as highlighted in figure 11, represents extreme cases of incoming turbulence intensity. PDFs for this group are left-tail dominant indicating the dominance of extreme detrainment events. Even though a slight increase in the right hand side of the PDF is observed, it is far outweighed by large detrainment events, leading to a severely negative net entrainment into the wake. The PDF behaviour is indicative of a high level of intermittency, which is expected given the incoming free-stream turbulence conditions (this is discussed to a greater extent in the following paragraph). Group 2 presents a slight loss in entrainment, however, the cylinder wake still has a positive mean net entrainment mass flux. Behaviour in this group is characterised by both a slight suppression of the right tail as well as a slight increase in the detrainment side of the PDF. This behaviour provides a negative skewness value and hence, a lowered net entrainment flux into the wake. Group 1 consists of cases that provide a low amount of incoming free-stream turbulence intensity, including the no-grid case. A positive value for skewness followed by a net positive entrainment mass flux into the wake, define this group's characteristics.

Runs 7, 19 & 20 display a negative mean entrainment flux, suggesting a net loss of mass from the wake to the background. This remains a physical result as the geometry of these cases, place the field of view in a region that investigates the interaction between two strong wakes. Figure 14 displays the turbulence intensity profile downstream of the regular grid as well as the location of the field of view for runs 19 & 20. All three cases are in the near vicinity ($x/L_0 < 7$) of a regular square grid, meaning that the wakes shed from the bars of the regular grid have a turbulence intensity that is greater than that of the cylinder wake. Hence, the FOV investigates a region where two wakes are com-

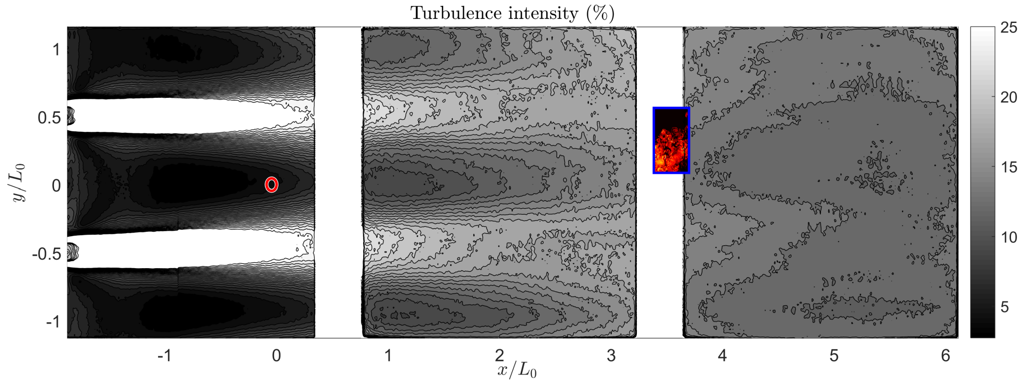

Figure 14: Turbulence intensity profile downstream of a square regular grid with $L_0 = 111$ mm. The overlay represents the investigated FOV. The positioning of the grid, cylinder and the experimental FOV is consistent with that of runs 19 & 20.

peting against each other to entrain fluid from one and another. A process such as this is highly intermittent (c.f. Baj & Buxton (2019)) and results in much greater variation of mean flux. It is possible that the net entrainment result is largely influenced by the phase correlation of the two shed wakes. This suggests a larger number of shedding cycles need to be experimentally captured in order to attain convergence. Furthermore, the role of the turbulence intensity level in the wake could be to act as a critical point, beyond which a net mass detrainment is possible.

The behaviour of flux with respect to subjected length scale is much less clear and is seen as a secondary parameter with regards to its influence on entrainment flux. The lack of correlation is evident in figure 12.

Turbulence paramter

Several investigators in the past have used the turbulence parameter in an attempt to reconcile the effects of both length scale and turbulence intensity in a single form. A slightly modified version of the original parameter initially used by Taylor (1936), is presented in equation (4).

$$T_p = (TI)^m \left(\frac{L_{12}}{d}\right)^n \tag{4}$$

Running an optimisation algorithm to calculate the best linear correlation between T_p and mean normalised flux, produces the coefficients, $m = 1.49$ & $n = -0.39$. An increase of 12.6% in the coefficient of determination is achieved when comparing it to a linear fit based on the turbulence intensity alone. The optimal coefficients clearly encourage the influence TI, whilst providing a slight inverse correlation to L_{12}.

CONCLUSION

The effects of length scale and turbulence intensity in the background turbulence were evaluated using simultaneous PIV and PLIF experiments conducted in the far wake of a circular cylinder. The classical result of an enstrophy jump at the interface can still be seen when turbulent rotational fluid is available on both sides of the interface. Additionally, background turbulence does act to increase the shear rate at the interface. Furthermore, it was found that the entrainment process is largely sensitive to turbulence intensity of the incoming grid turbulence. Despite the presence of background turbulence leading to an increase of interface surface area, a net reduction in entrainment flux is observed with increased background turbulence intensity. This is mainly due to the action of large, but infrequent detrainment events that reside in the left tail of the mass flux PDF. In the most extreme case, where, the background itself consisted of a strong wake, net detrainment was found to occur. Finally, an attempt to collectively analyse the effects of length scale and turbulence instensity through the use of the turbulence parameter, resulted in power coefficients that promoted the influence of TI, whilst being inversely correlated to a slight extent to L_{12}.

REFERENCES

Baj, P., Bruce, P.J.K. & Buxton, O.R.H. 2016 On a PLIF quantification methodology in a nonlinear dye response regime. *Experiments in Fluids* **57** (6), 1–19.

Baj, P. & Buxton, O.R.H. 2019 Passive scalar dispersion in the near wake of a multi-scale array of rectangular cylinders. *Journal of Fluid Mechanics* **864**, 181220.

Ching, C.Y., Fernando, H.J.S. & Robles, A. 1995 Breakdown of line plumes in turbulent environments. *Journal of Geophysical Research: Oceans* **100** (C3), 4707–4713.

Corrsin, S. & Kistler, A. L. 1955 Free-stream boundaries of turbulent flows. *NACA technical report* (1244).

Eames, I., Jonsson, C. & Johnson, P.B. 2011 The growth of a cylinder wake in turbulent flow. *Journal of Turbulence* (12), N39.

Gaskin, S.J., McKernan, M. & Xue, F. 2004 The effect of background turbulence on jet entrainment: an experimental study of a plane jet in a shallow coflow. *Journal of Hydraulic Research* **42** (5), 533–542.

Holzner, M. & Lüthi, B. 2011 Laminar superlayer at the turbulence boundary. *Physical Review Letters* **106** (13), 134503.

Mistry, D., Philip, J., Dawson, J.R. & Marusic, I. 2016 Entrainment at multi-scales across the turbulent/non-turbulent interface in an axisymmetric jet. *Journal of Fluid Mechanics* **802**, 690–725.

da Silva, C.B., Hunt, J.C.R., Eames, I. & Westerweel, J. 2014 Interfacial Layers Between Regions of Different Turbulence Intensity. *Annual Review of Fluid Mechanics* **46** (1), 567–590.

Taylor, G. I. 1936 Statistical Theory of Turbulence V Effect of Turbulence on Boundary Layer Theoretical Discussion of Relationship Between Scale of Turbulence and Critical Resistance of Spheres. *Proceedings of the Royal Society of London* **156** (888), 307–317.